Journal of Applied Polymer Science

Viscoelastic properties of poly(ε-caprolactone)/clay nanocomposites in solid and in melt state

Marija S. Nikolic,[1] Miodrag Mitric,[2] Aleksandra Dapcevic,[1] Jasna Djonlagic[1]

[1]Faculty of Technology and Metallurgy, Department of General and Inorganic Chemistry, University of Belgrade, Belgrade, Serbia
[2]Vinca Institute of Nuclear Sciences, Laboratory for Theoretical and Condensed Matter Physics, University of Belgrade, Belgrade, Serbia
Correspondence to: M. S. Nikolic (E-mail: mnikolic@tmf.bg.ac.rs)

ABSTRACT: Viscoelastic properties in solid and in melt state of poly(ε-caprolactone), PCL, nanocomposites with organomodified clays (Cloisite30B and Cloisite15A) are thoroughly investigated. Although WAXD is insensitive to the difference in the nanocomposites structure, the melt rheology reveals pronounced differences between the two series. Melt yield stress values, obtained from fittings by the Carreau–Yasuda model, are used as a measure of partial exfoliation of the clay. Temperature dependence of the shift factors, used for time–temperature superposition of the modulus curves, yields similar values of the flow activation energies for all the samples. Temperature dependences of the dynamic modulus and loss factor of solid nanocomposites were correlated to the structural differences deduced from the melt rheology. The increase in the storage modulus is compared to the theoretical predictions from the Halpin–Tsai model. The effective aspect ratio obtained from this comparison agrees reasonably with the value estimated from the melt rheology. © 2015 Wiley Periodicals, Inc. J. Appl. Polym. Sci. **2016**, *133*, 42896.

KEYWORDS: biodegradable; clay; polyesters; viscoelasticity; viscosity

Received 9 June 2015; accepted 29 August 2015
DOI: 10.1002/app.42896

INTRODUCTION

Poly(ε-caprolactone), PCL, biodegradable and biocompatible polyester has received a renewed attention as a potential biomaterial and alternative to conventional non-biodegradable plastic materials.[1] PCL is semicrystalline polyester with mechanical performances comparable to low density polyethylene, good processability, and compatibility with many other polymers. Along with the research on the potential applications of PCL, the very intensive field of current research is the improvement of its mechanical properties. The poor mechanical and barrier properties of this polyester were found to be the main drawbacks in many applications related to the biomedical field and packaging. These properties of PCL can be improved by the incorporation of nanofillers, where special interest is in the natural layered silicates, that is, clays.[2–5] Nanocomposites of PCL with various organomodified nanoclays have been obtained through solvent casting method, melt processing and *in situ* intercalative polymerization.[6–11] Various properties of PCL based nanocomposites have been investigated, including mechanical, thermal, barrier as well as biodegradability potential.[7,12–15] There is also an interest in studying the viscoelastic properties of the PCL based nanocomposites, in both solid and melt state, with the attempt to correlate them with the final dispersion state of the nanofiller and its impact on overall performance of the nanocomposite.

The viscoelastic properties of the nanocomposites in solid and melt state are related to the processing and application aspects. Also, the melt rheology parameters can be used to get insight into the structure of composites filled with different nanofillers, such as silica nanoparticles, carbon nanotubes, or layered silicates. Viscoelastic properties of the composites in the melt state are sensitive to the particle size, shape, and its interaction with polymer matrix, which can be dictated through the surface chemistry of the filler.[16,17] The higher melt viscosities, shear-thinning, and non-terminal response in the low frequency region are usually observed in the low amplitude shear measurements. This transition from liquid to solid-like response of the melt is usually ascribed to the formation of a filler network. The rheological percolation threshold can be deduced from the increase in the low-frequency modulus with increasing nanofiller volume fraction.[18–20] The melt rheology of the PCL nanocomposites has been investigated in a number of studies, where these nanocomposite even served as a model system to investigate the potential of rheological studies in the determination of the nanocomposite microstructure.[21] The melt rheology is a powerful tool in the investigation of the dispersion level of the clay as proven in a several studies.[21–25] Using a PCL/Cloisite30B as a model system Van Assche *et al.* have proposed a combination of the time–temperature superposition principle (TTS), and zero-shear modulus corrected Carreau–Yasuda model to

Table I. Composition, Degrees of Crystallinity, and Melting Temperatures of the Nanocomposites

Sample	Type of clay	Organoclay content (wt %)[a]	ϕ (vol %)[b]	$X_{c(WAXD)}$ (%)[c]	$X_{c(DSC)}$ (%)[d]	T_m (°C)[d]
PCL	/	/	/	66.0	60.2	74
PCL/C30B-1	Cloisite®30B	1.0 (0.7)	0.6	55.0	53.4	71
PCL/C30B-3		3.0 (2.2)	1.8	52.2	59.7	72
PCL/C30B-5		5.0 (3.6)	2.9	52.5	54.4	71
PCL/C30B-8		8.0 (5.8)	4.6	47.2	53.2	71
PCL/C15A-1	Cloisite®15A	1.0 (0.6)	0.7	51.4	56.3	72
PCL/C15A-3		3.0 (1.8)	2.1	56.6	54.0	71
PCL/C15A-5		5.0 (2.9)	3.5	46.9	57.6	72
PCL/C15A-8		8.0 (4.6)	5.5	43.0	53.3	70

[a] Values in the brackets refer to inorganic part.
[b] The volume fraction of the clay calculated using the following values of the densities of the composite constituents: $\rho_{PCL} = 1.2$ g/cm^3, $\rho_{C30B} = 1.98$ g/cm^3, $\rho_{C15A} = 1.66$ g/cm^3.
[c] Determined from WAXD measurements.
[d] Determined from DSC measurements.

quantify the dispersion level of the clay in the matrix.[26] Melt rheology was used to detect rheological percolation of different PCL based nanocomposites. Yi Li *et al.* determined a rheological percolation threshold for the PCL/silica nanocomposites to be between 7 and 9 wt % of silica nanoparticles, which is higher compared to PCL/clay and PCL/carbon nanotube nanocomposites—expected result taking into account the high aspect ratio of the later fillers.[18] Temperature effects induced in the nanocomposites' melts were also studied by melt rheology. For nanocomposites of PCL with multi-walled carbon nanotubes Wu *et al.* have observed a temperature dependence of the percolation network by analyzing Han plots of G' versus G'' obtained at different temperatures, where TTS principle could not be applied.[27] Similarly, in the case of an intercalated system of PCL/Cloisite30B nanocomposite, Kwak *et al.* observed a temperature induced morphological changes which were not present in the exfoliated system to which TTS was applicable.[28] Ahmed *et al.* have shown a failure in the TTS principle for PCL/Cloisite30B nanocomposites prepared by solution casting.[29] The variations in the preparation method and chosen conditions, as well as the structural diversity of the nanocomposites, impose the necessity of studying the each system individually.

Dynamic–mechanical analysis in the solid state (DMA) can give further insight into the structure of the nanocomposite. Although, there are a lot of studies in which DMA is used to characterize the mechanical performance of the PCL based nanocomposite,[6,30–32] there are a few studies which try to directly link the parameters obtained in the investigations of the viscoelastic behavior of the material in solid and in melt state.

In this study, nanocomposites of PCL with two types of organomodified clays were prepared and their melt rheological behavior was studied. The state of dispersion of the organomodified clay was estimated from the rheological measurements in conjecture to different composition of organomodified clays. In addition the viscoelastic properties in the solid state were evaluated and the performance in terms of the mechanical properties of two different nanocomposites was compared. Finally, structural characteristics of the nanocomposites deduced from the dynamic measurements in melt state and in solid state are compared.

EXPERIMENTAL

Materials

Poly(ε-caprolactone) was synthesized by the ring-opening polymerization of ε-caprolactone with tin-2-ethylhexanoate as the catalyst. The polymerization was performed in a bulk for 3 h at 180°C under nitrogen. The polymer was dissolved in chloroform, precipitated into cold methanol, and dried under vacuum at room temperature. The number average molecular weight obtained from gel-permeation chromatography measurements was 43,300 g/mol, with a polydispersity of 1.95. The organomodified clays were provided from Southern Clay (TX). The organoclay Cloisite®30B (C30B) possess methyl bis-2-hydroxyethyl tallow quaternary ammonium cation and organoclay Cloisite®15A (C15A) possess dimethyl dehydrogenated tallow quaternary ammonium cation as organic modifier. All solvents used were purchased from Merck and Aldrich and were used as received.

Nanocomposites Preparation

Nanocomposites were prepared by solution casting method from chloroform, as explained in detail elsewhere.[33] The starting dispersion of the clay (1 wt %) was added to the chloroform solution of PCL (6 wt %) in predetermined amount, so as to get the nanocomposites with 1, 3, 5, and 8 wt % of the clay. The prepared dispersions were poured into the Petri dishes. The chloroform was allowed to evaporate under ambient conditions resulting in uniform and compact films of the thickness between 150 and 200 μm. The samples' designation and composition are given in Table I.

Wide Angle X-ray Diffraction

The wide angle X-ray diffraction (WAXD) patterns were obtained from Philips PW 1050 powder diffractometer with Ni filtered CuK_α radiation ($\lambda = 1.5418$ Å) and scintillation detector.

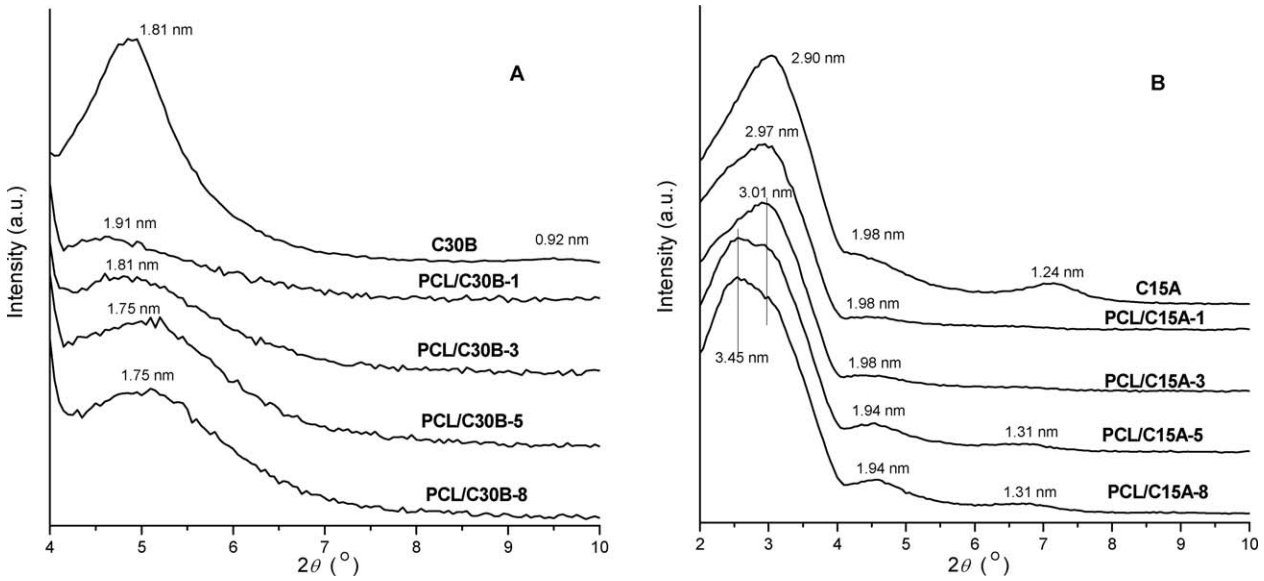

Figure 1. WAXD patterns of organomodified clays and nanocomposites up to $2\theta = 10°$ (A) C30B series and (B) C15A series.

Diffraction data were collected within 2–35° 2θ range in steps of 0.05°, and scanning time of 10 s per step.

WAXD measurements were conducted on the compression molded samples prepared for the dynamic mechanical analysis. Prior to the measurements, the samples were stored at room temperature in closed containers. The degree of crystallinity was calculated from the areas of amorphous halo and the all crystalline peaks, which were determined by deconvoluting the patterns to the sum of Voight functions by using the PeakFit® program.

Differential Scanning Calorimetry

Differential scanning calorimetry (DSC) measurements were performed on an SDT Q600 (TA Instruments) instrument. The samples (around 7–8 mg) were scanned from 30 to 120°C at a rate of 10°C/min in a nitrogen atmosphere (flow rate: 100 cm^3/min). DSC measurements were conducted on the compression molded samples prepared for the dynamic mechanical analysis. From DSC traces the melting temperatures were determined as a temperature of the peak maximum, while degrees of crystallinity were calculated from corresponding enthalpies of melting normalized to the PCL content by comparing them to the theoretical (136.1 J/g)[14] value of enthalpy of melting for 100% crystalline PCL.

Melt Rheology

Rheological measurements in the melt were conducted on a Discovery Hybrid Rheometer HR2, TA Instruments. Dynamic oscillatory shear measurements were performed between parallel plates with a diameter of 25 mm, while the thickness of the samples was around 1 mm. Frequency sweep tests were performed in the temperature range from 80 to 120°C. The angular frequency was varied from 0.1 to 100 rad/s with five points per decade on the logarithmic scale. The strain amplitude was kept constant at 1%, which was checked to be in the linear viscoelastic range. The samples for rheological investigation were prepared by compression molding at 75°C using a hydraulic press to obtain discs with a diameter of 25 mm.

Dynamic Mechanical Analysis in Solid State

Dynamic mechanical properties in solid state were also investigated on the Discovery Hybrid Rheometer HR2, TA Instruments, in the torsion mode with a static pre-tension of 1 N. The temperature sweeps at a fixed frequency of 6.28 rad/s were performed in the temperature range from −100 to 60°C. The strain amplitude was 0.1% and the temperature step was 2.5°C. The size of the test samples was 40 × 12 × 1 mm^3.

RESULTS AND DISSCUSION

WAXD Characterization

In Figure 1, WAXD patterns of PCL nanocomposites of the two series and the corresponding clays are presented, in the 2θ range where the appearance of the reflection of the characteristic (0 0 1) plane of the clays is expected. Characteristic d-spacing calculated from the position of the observed peaks is also indicated in Figure 1. In the pattern of the C30B clay two diffraction peaks are observed at $2\theta = 4.9°$ ($d_{001} = 1.81$ nm) and $2\theta = 9.6°$ ($d_{002} = 0.92$ nm). For the nanocomposite with the lowest content of the clay in the first series (PCL/C30B) a slight shift of the (0 0 1) reflection to the lower 2θ (higher d-spacing) is observed. The change is very small and cannot be taken as an indication of the intercalation, as the minimum expected expansion of the d-spacing would be at least 0.4 nm, in the case of a planar monolayer of the PCL macromolecules.[34] For the higher clay loadings the gradual shift of the peak maximum toward higher 2θ is observed, with characteristic d-spacing changing from 1.81 to 1.75 nm. This might be an indication of the partial collapse of the clay structure or rearrangement of the surfactant molecules. At the same time, the broadness of the peaks is a hint that a distribution of clay interlayer distances exists in the nanocomposites. Overall the subtle changes in the (0 0 1) reflection position suggest that there is no appreciable change in the

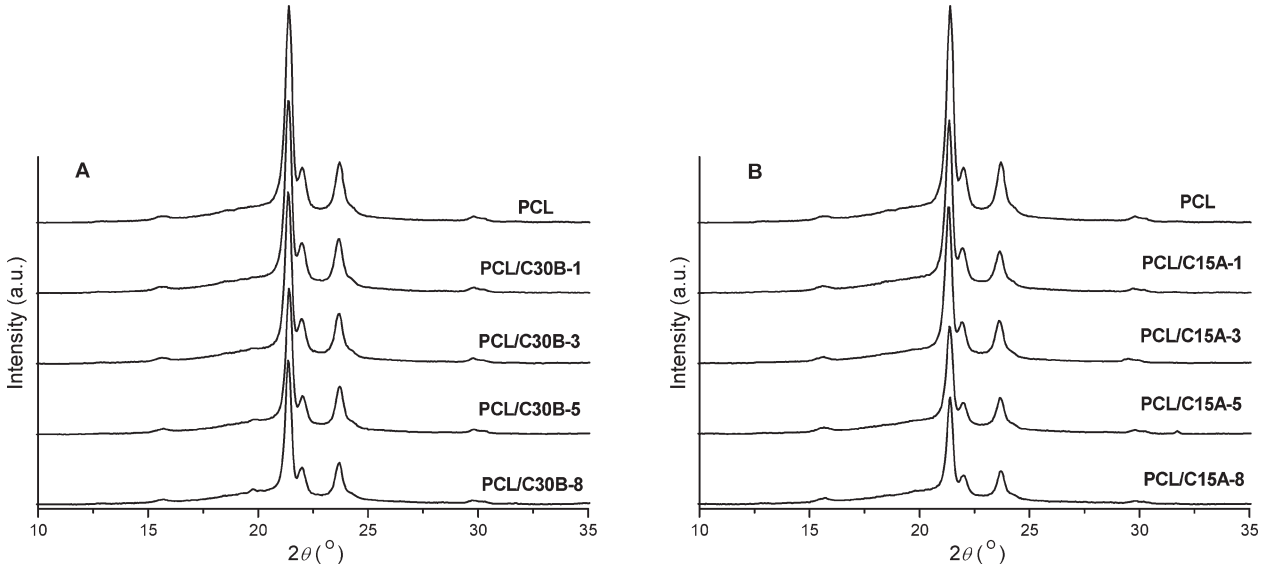

Figure 2. WAXD patterns of PCL and its nanocomposites in the 2θ range from 10 to 35° (A) C30B series and (B) C15A series.

clay structure, that is, the clay tactoids present in the nanocomposite mostly have an unaltered basal spacing.

In the second series [Figure 1(B)] the peak corresponding to the reflection from (0 0 1) plane of the organomodified C15A clay is positioned at $2\theta = 3.04°$ giving an interlayer distance of $d_{001} = 2.90$ nm in the pure clay. The (0 0 2) reflection at $2\theta = 7.11°$ ($d_{002} = 1.24$ nm) is also visible in this pattern. The peak appearing at $2\theta = 4.46°$, which does not change its position within the nanocomposite series is an indication of the structural inhomogeneity of the C15A clay. Judging from the shape of the peak corresponding to the reflection from the (0 0 1) plane of the clay present in the nanocomposites the existence of an interlayer spacing distribution is more obvious in this series. In the patterns of the nanocomposites with C15A clay, besides the peak at around $2\theta = 3°$ (around 3 nm), a shoulder peak at lower 2θ of 2.56° (3.45 nm) appears, gradually increasing in intensity with the increase in the clay loading. WAXD patterns of nanocomposites in the both series could not give proof of the presence of a single type of the microstructure: intercalated or exfoliated, although there is an indication of a slightly favorable intercalation in the second series. As presented in a number of studies, WAXD alone cannot be used for the definite conclusion on the structure of nanocomposites, which may consist of original clay particles (tactoids), single dispersed layers, and intercalated clay tactoids with a distribution of interlayer distances, existing together in the nanocomposite.[21,22,35] In the both presented series it can be assumed that the nanocomposite structure consists of single clay layers (which are XRD silent) and layer stucks (tactoids) with interlayer distances as in the pure clay, the size of which may vary. A portion of the PCL intercalated clay in the second series may also be assumed. What will determine the properties of the nanocomposite is the effective aspect ratio of the nanofiller and possible percolation of the filler particles which cannot be probed by the WAXD.

Figure 2 presents WAXD patterns of PCL and its nanocomposites for 2θ above 10°, where crystalline reflections from the PCL crystalline phase are expected. As can be seen there is no change in the position of the reflections arising from the PCL crystalline phase, which in all nanocomposites appear at the expected position for the neat PCL matrix. The PCL crystallized in the α-form with characteristic reflections from (1 1 0), (1 1 1), and (2 0 0) appearing at 21°, 22°, and 24°, respectively.[36] The degrees of crystallinity obtained from these patterns are given in Table I. The degree of crystallinity of neat PCL is 66%. A decrease in the crystallinity is observed for the nanocomposites with the addition of the clay. From DSC measurements it was confirmed that the nanocomposites have lower degrees of crystallinity although with smaller difference compared to the homopolymer, and in less regular fashion with change in the clay content. At the same time DSC revealed a small decrease in melting temperatures of the nanocomposites (Table I). The incorporation of the nanofiller into the polymer matrix can enhance, retard, or even has no influence on the amount crystalline PCL fraction in the nanocomposites. The actual degree of crystallinity depends on the particular composite system and preparation procedure.[7,14,29,30,37,38] Lower degrees of crystallinity for prepared nanocomposites, as a consequence of the presence of the clay, will affect their solid state properties, such as barrier and mechanical properties.

Melt Rheology

The rheology of the PCL and nanocomposites' melt was investigated in low oscillatory shear experiments by performing frequency sweeps at different temperatures. The storage modulus and the complex viscosity dependences on angular frequency at 80°C for the two series are presented in Figure 3.

PCL melt exhibits a typical liquid-like behavior with pronounced Newtonian plateau and a slight shear-thinning at higher frequencies. With the addition of the clay the viscosity of the melt increases in the whole frequency region (with the exception of the PCL/C15A-8 sample with pronounced shear-thinning behavior at low frequencies). With the increase in the clay content, the Newtonian behavior is gradually converted to

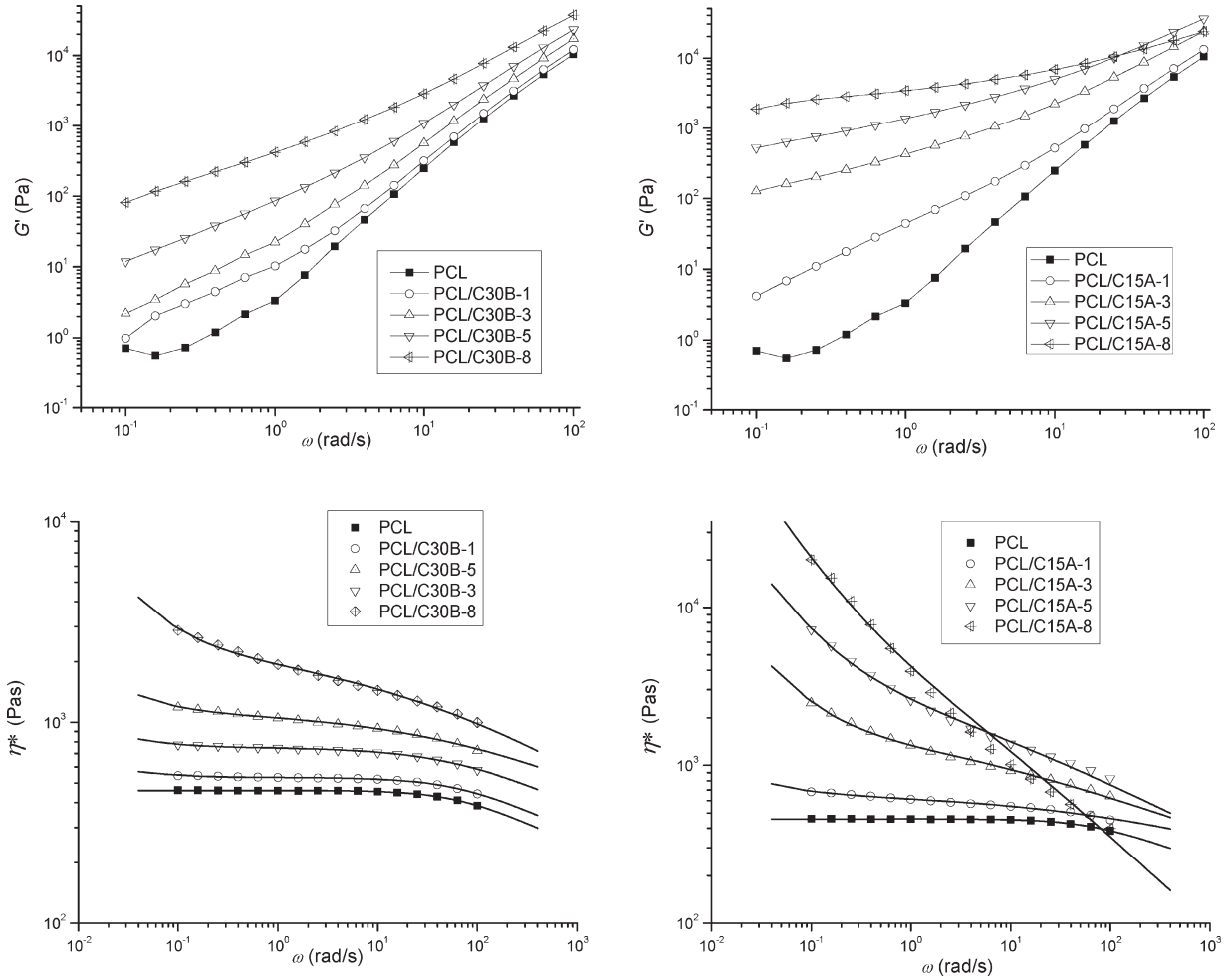

Figure 3. Storage modulus (G') and complex dynamic viscosity (η^*) frequency dependences at 80°C for PCL and its nanocomposites. The solid lines at $\eta^*(\omega)$ dependences present Carreau–Yasuda model fittings to the data.

the shear-thinning response at low frequencies. In the $G'(\omega)$ dependence deviation from the liquid-like behavior is obvious, where a gradual approach to the solid-like response of the melt can be observed. In the terminal zone, the power law dependences of $G' \sim \omega^2$ and $G'' \sim \omega^1$, expected for the pure homopolymer are not observed for nanocomposites. In Table II, the scaling exponents are summarized for all nanocomposites. For the PCL melt the deviation from the scaling exponent of 2 partially originates from the polydispersity of the polymer as well as from the transducer error as G' goes too low. For the nanocomposites, the scaling exponent steadily decreases with the increase in the clay loading in both series. A similar behavior is observed in the G'' frequency dependence (not presented) where the deviation from the scaling exponent of 1 is gradually increased. The deviation from the theoretical exponent in the power law dependences of $G'(\omega)$ and $G''(\omega)$ is more pronounced in the case of nanocomposites with C15A clay. This may lead to the conclusion that either a stronger network is formed or that the interaction between the clay particles and the matrix is stronger in this series.

The appearance of solid-like behavior is attributed to the formation of the percolating network of the clay particles (stuck of layers in the present nanocomposite system), which retard molecular relaxation of the polymer chain and possible interaction between the clay and the polymer matrix. The volume fraction of the clay at which the percolation appears was estimated

Table II. Low Frequency Scaling Exponents of $G'(\omega)$ and $G''(\omega)$ Measured at 80°C for PCL and Its Nanocomposites and Activation Energies Calculated from the Shift Factors

	Scaling exponent		
Sample	G'	G''	E_a (kJ/mol)
PCL	1.12	1.00	33.4
PCL/C30B-1	0.92	0.99	34.9
PCL/C30B-3	1.05	0.98	34.3
PCL/C30B-5	0.88	0.95	33.2
PCL/C30B-8	0.67	0.85	30.1
PCL/C15A-1	1.01	0.95	37.1
PCL/C15A-3	0.54	0.80	34.9
PCL/C15A-5	0.42	0.69	29.0
PCL/C15A-8	0.21	0.48	

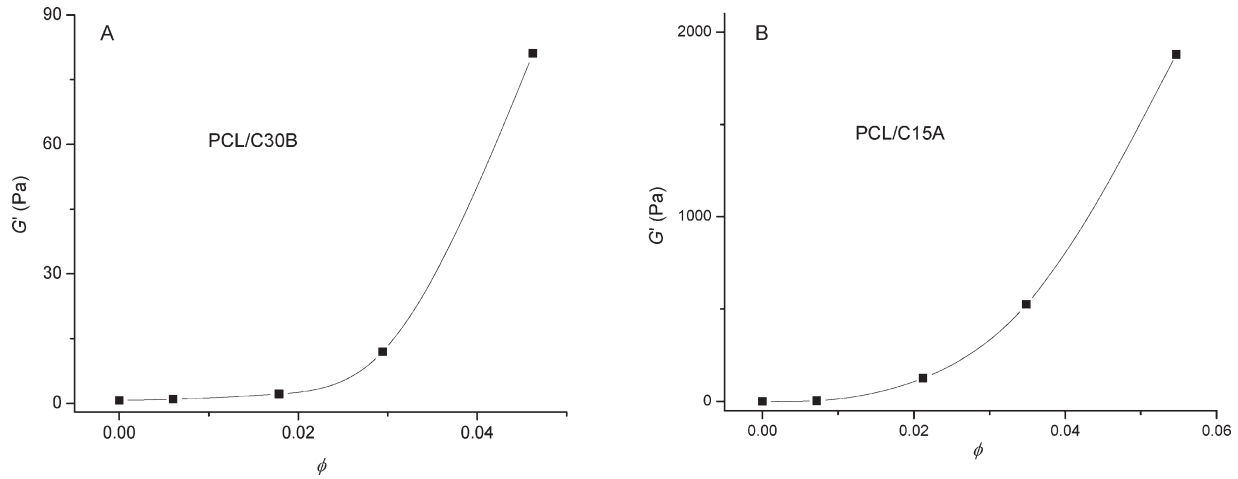

Figure 4. Dependence of the storage modulus measured at the lowest frequency at 80°C on the clay volume fraction for (A) C30B series and (B) C15A series.

from the plot of storage modulus at the lowest probed frequency as a function of the clay volume fraction (presented in Figure 4). The volume fraction of the clay at which abrupt change in the $G'(\phi)$ appears is around 0.02 for the both series and this can be taken as a percolation threshold of the clay particles. Above this critical value, G' increase exhibits a power low dependence on volume fraction of the clay with $G' \sim \phi^{3.8}$ for the C30B series and $G' \sim \phi^{3.0}$ for the C15A series. The obtained power law indices are around the values usually determined for the nanoclay composites.[23]

According to Ren *et al.* for the randomly oriented system the aspect ratio of the disc-shaped filler can be calculated from the determined percolation threshold volume fraction as:[39]

$$A_f = \frac{3\,\phi_s}{4\,\phi_p}, \tag{1}$$

where $A_f = l/t$ is the aspect ratio of the clay stuck (with the thickness t and the length l), $\phi_s = 0.3$ is the percolation threshold volume fraction for the randomly packed spheres and ϕ_p is the percolation threshold volume fraction of the clay particles. By taking the ϕ_p to be 0.02 the aspect ratio, A_f, of around 11 is obtained for the percolating clay particles. The obtained value is an effective aspect ratio, as the nanocomposite comprises of clay particles (tactoids) with different sizes and thicknesses, that is, there exists a distribution of the clay aspect ratios.

In further attempts to quantify the difference in the melt rheological response of the nanocomposites with different organo-modified clays, we focused on the difference in the low frequency complex viscosity. First introduced by Lertwimolnun for the clay-based nanocomposites,[40,41] the Carreau–Yasuda model, with a yield stress to account for the increase of the viscosity in the low frequency region, was used in the number of studies for the quantification of the dispersion quality of the clay:[42,43]

$$\eta*(\omega) = \frac{\sigma_0}{\omega} + \eta_0[1 + (\lambda\omega)^{\alpha}]^{(m-1)/\alpha}, \tag{2}$$

where σ_0 is the melt yield stress, η_0 is the zero shear viscosity, λ is the characteristic time constant, α is the Yasuda parameter, and m is the dimensionless power law index. The first term contains yield stress and was shown to correlate with exfoliation of the clay.

In the fitting procedure of this five-parameter model the viscosity curve of the neat PCL is first fitted by taking the σ_0 to be 0. For almost all nanocomposites, the behavior in the high frequency region seems to follow the same power law dependence, thus the power law exponent obtained for the PCL melt was kept constant for all the samples as long as the fitting gave the realistic results. The obtained fitting parameters are summarized in Table III and the corresponding fittings are presented in Figure 3, together with experimental data.

As can be seen in Figure 3 the obtained model curve captures the viscosity dependence very satisfactory. To get good fitting the power law index for the nanocomposite samples with higher clay loadings had to be adjusted to lower values than for the matrix. This can be an indication of the higher amount of the chains with restricted motions either through more developed clay network or by stronger interaction between the clay and the matrix. The change of the characteristic relaxation time and the Yasuda parameter is less regular. However, the constant increase in the relaxation time in the second series can be

Table III. Parameters of Carreau–Yasuda Model Used for Fitting the Complex Viscosity Frequency Dependence

Sample	σ_0 (Pa)	η_0 (Pa s)	λ (s)	α	m
PCL	0	459	0.0152	1.35	0.769
PCL/C30B-1	1.50	531	0.0149	1.20	0.769
PCL/C30B-3	3.15	748	0.0157	0.85	0.769
PCL/C30B-5	10.53	1122	0.0172	0.45	0.769
PCL/C30B-8	78.80	2500	0.0137	0.31	0.6110
PCL/C15A-1	4.63	673	0.00379	0.33	0.769
PCL/C15A-3	109.79	1600	0.4120	0.45	0.769
PCL/C15A-5	426.83	4883	1.0	0.31	0.648
PCL/C15A-8	1616.52	8000	1.5	0.42	0.4

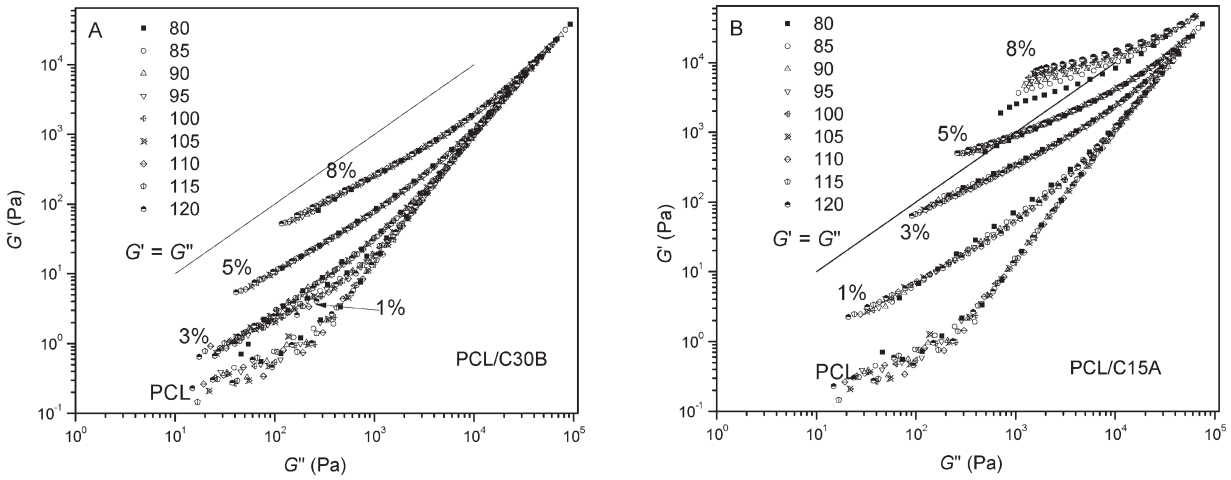

Figure 5. Han plots of the G' versus G'' at different temperatures for the PCL and its nanocomposites; (A) C30B series and (B) C15A series.

observed, with persistently higher values compared to the first series and ascribed to the restricted movements due to the more developed clay network in this case. The values of the zero shear viscosity regularly increase with clay loading in the both series. However, as previously suggested, it is rather difficult to interpret these results when there is a disappearance of the Newtonian plateau.[41,44] The most important parameter obtained from this model, yield stress, continuously increases and takes values from 1.5 to 78.8 Pa in the first and from 4.63 to 1617 Pa in the second series. Interpreted as an indicator of achieved clay dispersion (ultimately exfoliation), obtained values lead to the conclusion that the level of exfoliation is higher with the increase in the clay content for the both series. The more clay is present the amount of the dispersed clay platelets is higher. Although the increase is modest for the first series it is quite significant for the second series. The dramatic increase of the yield stress in the second series implies that there is a larger fraction of exfoliated clay layers in nanocomposites with C15A clay. These results, together with WAXD analysis which suggests the presence of clay particles with unaltered interlayer distance and similar effective aspect ratio determined from the low frequency storage modulus dependence on the volume fraction of the clay, lead to conclusion that the structure of obtained nanocomposites is highly complex. The higher amount of exfoliated clay layers in the second series shows that C15A clay can be better dispersed than C30B clay. The interaction between the polymer matrix and the organic modifier is more favorable in the case of the C30B clay, through possible interaction of the carbonyl group of PCL and the hydroxyl group of organic modifier. However, the dispersant used for the nanocomposite preparation has better swelling capability for the C15A clay and aids to the amount of the fraction of the exfoliated clay in this case.

Temperature Dependences

Structural differences between the nanocomposites with different fillers are very often deduced using Han plots (modified Cole–Cole plots) of storage versus loss modulus with a frequency as a parameter. Figure 5 presents the G' versus G'' dependence at different temperatures. The curves for the different nanocomposites taken at the same temperature do not fall on the same line, which indicate a structural difference among the samples within the same series as well as between the two series. A gradual increase in the slope of the curves for different samples can be observed. G' value for the given G'' is increasing, being higher than G'' for the higher clay contents, above 5 wt % in the first and 3 wt % in the second series. Besides the observation of the microstructural changes at fixed temperature, Han plots were also used to observe possible structural changes with temperature. If the curves of G' versus G'' coincide for different temperatures, it is assumed that the microstructure does not change with temperature, as in the single-phase melt. It is obvious that for the investigated nanocomposites in the temperature range from 80 to 120°C microstructural changes do not take place. The exception is the nanocomposite with the highest content of the C15A clay where the change in the microstructure with temperature can be deduced from the upward shift of the G' versus G'' curves with change in the temperature. Similar temperature induced changes in the nanocomposite structure has been explained by the dynamic percolation structure or by the enhanced dispersion of the clay induced by temperature changes during the tests.[28,45] For this sample, it can be assumed that by changing the temperature, the characteristic relaxation times are not only temperature dependant, but also become a structure dependant and, as presented in other studies, such nanocomposites do not obey a time–temperature superposition principle.[27,28,46] Therefore, this sample was excluded from subsequent TTS analysis.

The measurements performed at temperatures from 80 to 120°C were superimposed at reference temperature of 100°C by applying a time–temperature superposition and obtained master curves for storage modulus frequency dependence are presented in the Figure 6.

As predicted from the analysis of the Han plots, the nanocomposites obeyed the time–temperature superposition principle showing thermorheological simplicity. The good superposition was achieved by applying a horizontal shift (a_T) of the G' curves, without a need to apply a vertical shift of the modulus

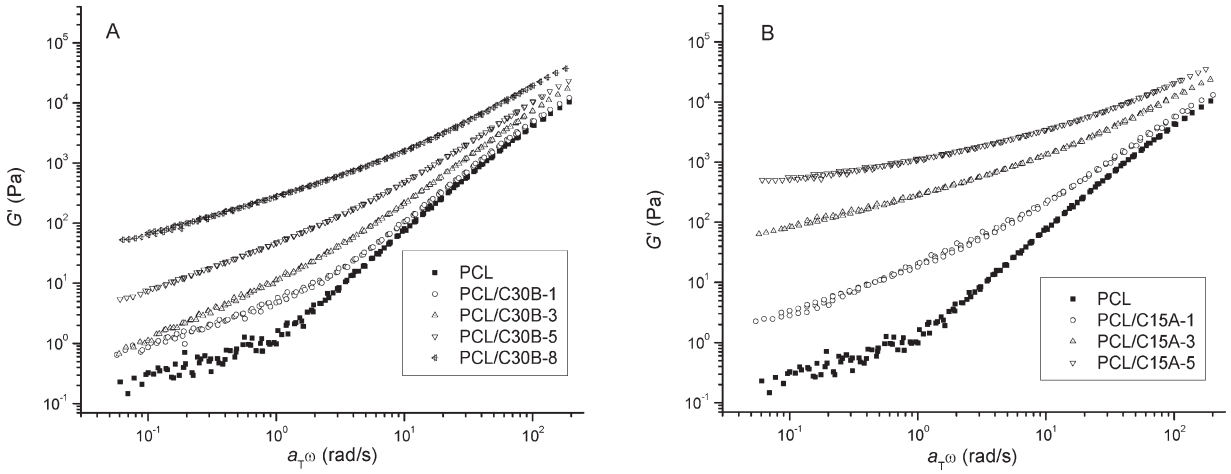

Figure 6. Master curves of the storage modulus frequency dependence at 100°C generated by using the time–temperature superposition for PCL and its nanocomposites; (A) C30B series and (B) C15A series.

curves. The temperature dependence of the shift factors for different nanocomposites is presented in Figure 7.

Applied frequency shift factors are relatively small and comparable to reported values for pure PCL and its various nanocomposites in the similar temperature window.[17,29,47,48] The shift factors used to obtain good superposition for the nanocomposites seem to be independent of the clay loading. The independence of shift factors on the type and the amount of clay, as previously observed, indicate that the relaxation processes taking place in the nanocomposites originate from the unaltered polymer matrix. As deduced from the WAXD a portion of the polymer matrix might be involved in the formation of the intercalated structure, for which different relaxation processes can be presumed. From the composition independence of the shift factors, it is expected that only a small portion of the polymer matrix is involved in the formation of an intercalated structure with altered relaxation properties. By applying an Arrhenius fit to the values of a_T at different temperatures, activation energies of flow were obtained (Table II). The value of

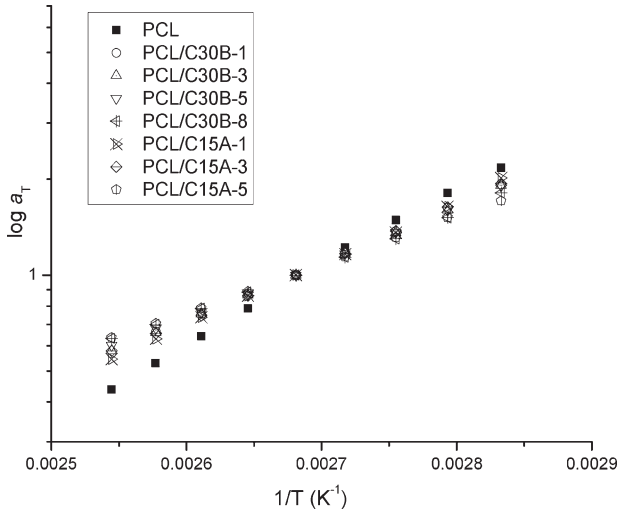

Figure 7. Temperature dependence of the shift factors for PCL and its various nanocomposites.

E_a for the pure PCL of 33.4 kJ/mol is in agreement with previously obtained values for PCL of different molecular weight.[47,49,50] The values for E_a obtained for nanocomposites are scattered and do not show any trend with the change of the clay content or the clay type, as sometimes observed for different PCL nanocomposites.[17,51] There are reports showing that flow activation energies are higher for the nanocomposites with proven intercalated structure, compared to the neat polymer. As the presented results show an independence or even slight decrease of flow activation energies for the nanocomposite, we can indirectly conclude that the portion of the intercalated structure is not significant.[52,53]

Dynamic Mechanical Analysis

Dynamic properties of the solid nanocomposites were studied by dynamic mechanical analysis in isochronal experiments at 6.28 rad/s. A variation of the storage modulus (G'), loss modulus (G''), and loss factor (tan δ) with the temperature are presented in Figures 8 and 9.

Loss factor as a function of the temperature displays a broad α-peak at around—50°C associated with cooperative motion of polyesters chain segments. At around −100°C, the appearance of a peak in tan δ curve is observed, which corresponds to β-relaxation, attributed to the in-chain rotations of the polymer constituent groups, taking place in the amorphous phase of PCL. The peak is not captured as a whole; however, it seems that the position and the height of this peak do not change considerably within the series. Conversely, the position, the height, and the width of the α-peak (values are summarized in Table IV) are all influenced by the presence, the amount, and the type of the organomodified clay. The glass transition temperatures, T_g, are taken as the temperature of the α-peak maximum in tan δ curves. Compared to the neat polymer, a slight shift in T_g values toward lower temperatures is observed for all nanocomposites, which can be explained with reduced crystallinity (as observed in the investigation of dynamic mechanical properties of PCL with varying degree of crystallinity[54]) or by the plasticizing effect of the organomodifier.[55,56] The differences in the area and the height of the α-peak between the two series

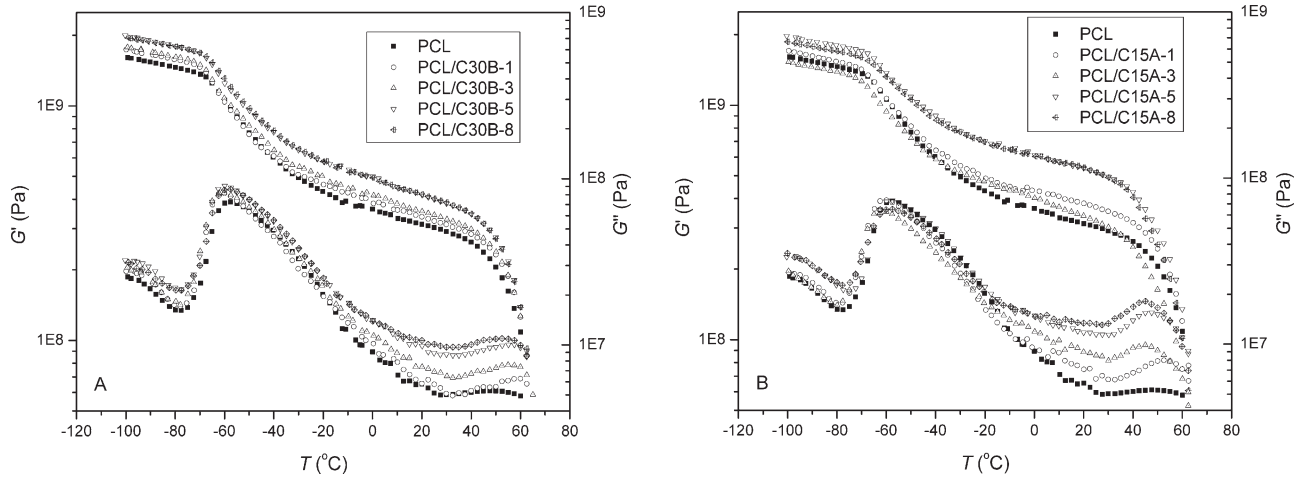

Figure 8. Variation of the storage and loss modulus with the temperature at 6.28 rad/s for the PCL and its nanocomposites; (A) C30B series and (B) C15A series.

are more pronounced. With the increase in the clay content the height and the area of the α-peak decrease, especially in the PCL/C15A series. The decrease in crystallinity, that is, the increase in the amorphous phase content, as an origin of this relaxation process, should produce quite opposite effect. Thus, the lowering of this peak, observed for the nanocomposites, is a consequence of the presence of the clay particles. The decrease in the peak height and the area point to the smaller amount of mobile matrix phase, as a consequence of an increase in the amount of constrained chains which are close to the clay surface.[57] The more pronounced decrease observed for the series with C15A is in a line with conclusion deduced from the viscosity curves that in the nanocomposites with this clay, amount of the exfoliated clay layers is higher.

In the loss modulus temperature dependence, between T_g and T_m the presence of the clay increases the values of G'' and consequently the damping effect is more pronounced. This effect is often observed for nanocomposites with various matrices and fillers as well.[31,52,58,59] Besides the main peak associated with α-transition, in G'' curves, the nanocomposites with C15A exhibit an additional peak in the high temperature region (around 45°C). Earlier investigations have ascribed the appearance of such peak to the molecular relaxations inside PCL crystallites formed under the influence of the clay.[6] As this peak in G'' curves is well resolved only for the series with C15A clay, it can be speculated that besides the difference in the clay state of dispersion between the two series of the nanocomposites, there is also a different distribution of clay platelets/tactoids among crystalline and amorphous phase.

The curves of the storage modulus temperature dependence for the nanocomposites of the both series lie above the curve for the matrix material in the whole investigated temperature region. Exception is the sample PCL/C15A-3, which shows modulus in the glassy state, even lower than neat PCL, without any apparent reason. The values of the storage modulus at—90, 0, and 20°C are listed in Table IV. The enhancement of the modulus is more pronounced above T_g for the both series. The relative increase in the modulus goes from 1.08 up to 1.24 for

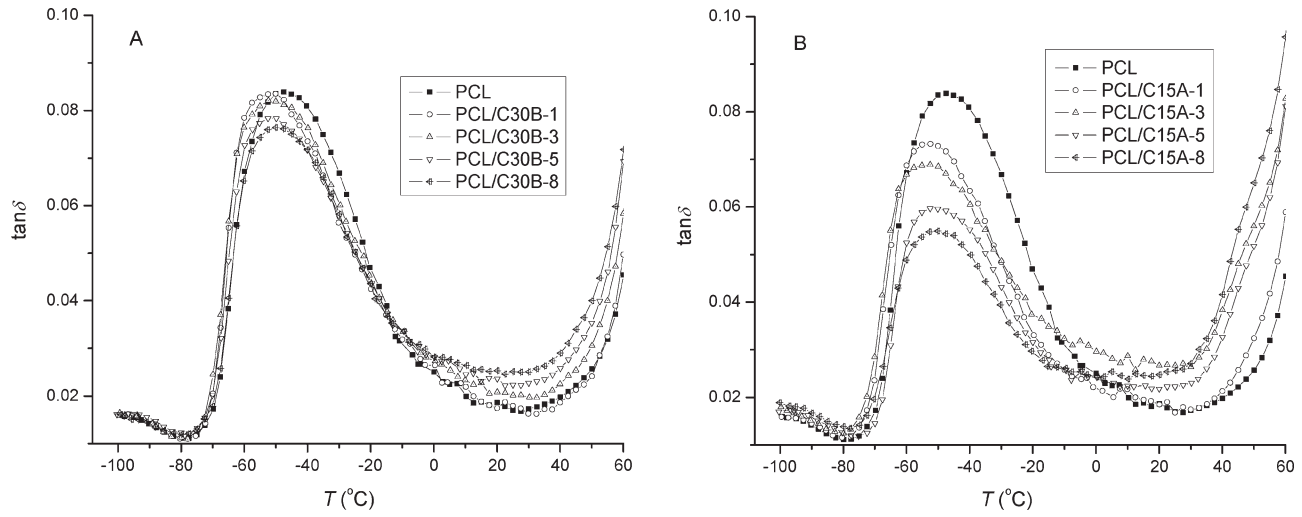

Figure 9. Loss factor as a function of temperature at 6.28 rad/s for the PCL and its nanocomposites; (A) C30B series and (B) C15A series.

Table IV. Storage Modulus at Different Temperatures and 6.28 rad/s, Glass Transition Temperatures, Height, and Width of α-Peak in tan δ Curves for PCL and Various Nanocomposites

					α-peak	
Sample	G' (−90°C) (GPa)	G' (0°C) (GPa)	G' (40°C) (GPa)	T_g (°C)	$(\tan\delta)_{height}$	$(\tan\delta)_{area}$
PCL	1.53	0.36	0.26	−48	0.084	33.7
PCL/C30B-1	1.66	0.39	0.28	−50	0.084	33.5
PCL/C30B-3	1.70	0.42	0.30	−52	0.082	33.8
PCL/C30B-5	1.90	0.50	0.34	−52	0.078	30.3
PCL/C30B-8	1.87	0.49	0.34	−50	0.076	29.5
PCL/C15A-1	1.62	0.43	0.32	−52	0.073	31.5
PCL/C15A-3	1.46	0.40	0.25	−44	0.069	27.1
PCL/C15A-5	1.87	0.61	0.43	−52	0.060	23.4
PCL/C15A-8	1.78	0.61	0.40	−50	0.055	21.1

the first series and from 1.06 to 1.22 for the second series in the glassy state. In the rubbery zone, the reinforcement ratio goes from 1.08 up to 1.39 for the first and from the 1.19 up to 1.69 for the second series. The similar trend is observed also at higher temperature of 40°C. This behavior is similar to the number of polyester/nanoclay systems where similar increments in G' are observed below and above T_g.

Improvements in the storage modulus can be modeled with Halpin–Tsai semi-empirical model widely used to predict the mechanical properties of nanocomposites reinforced with different fillers.[52,60–63] The measured storage modulus at 0°C is compared to theoretically predicted values obtained from the Halpin–Tsai model for platelet-like particles with two fitting parameters: filler loading and its aspect ratio. Halpin–Tsai expression for platelet reinforcement used was:

$$\frac{G'_{\text{nano}}}{G'_m} = \frac{1+A_f\eta\phi}{1-\eta\phi}, \tag{3}$$

where

$$\eta = \frac{(G'_{\text{clay}}/G'_m)-1}{(G'_{\text{clay}}/G'_m)+A_f}. \tag{4}$$

In the preceding expressions, G'_{nano}, G'_m, and G'_{clay} are the storage modulus of the nanocomposite, PCL matrix, and clay, respectively, ϕ is the volume fraction of the clay (Table I), and $A_f = l/t$ is the aspect ratio of the clay particles. By taking the G'_{clay} to be equal to 170 GPa,[52] model curves of the relative modulus as a function of the clay volume fraction for the different aspect ratios were obtained.

In Figure 10, the experimental and theoretical values obtained for the different aspect ratios are compared. For the highest clay content the relative modulus in the both series decrease. This may be an indication of the morphological irregularities induced with higher clay content, such as the formation of larger agglomerate or inhomogeneous dispersion of the clay particles. Experimental values do not strictly follow any of the theoretical curves. Apart from the values for the highest clay content, for the series with C30B clay, the experimental values are situated mostly around the curve obtained for the aspect ratio of 10, while the experimental values for the C15A series better follow the theoretical predictions obtained for the slightly higher aspect ratio. The obtained aspect ratios of the clay tactoids agree well with the value calculated from the melt rheological data ($A_f = 11$). The observed increase in the melt viscosity, giving rise to the solid-like behavior and high values of the yield stress, is a consequence of the small amount of the exfoliated clay in the C15A series. Although these exfoliated clay platelets have pronounced effect on the melt viscosity, they do not contribute significantly to the mechanical reinforcement. It can be concluded that the mechanical properties are more sensitive to the effective aspect ratio of the clay particles (tactoids) and the modulus of the composite components.

CONCLUSION

In this study, the dynamic viscoelastic properties in the melt and in the solid state, of nanocomposites with poly(ε-caprolactone) and organomodified clay, were investigated. The PCL

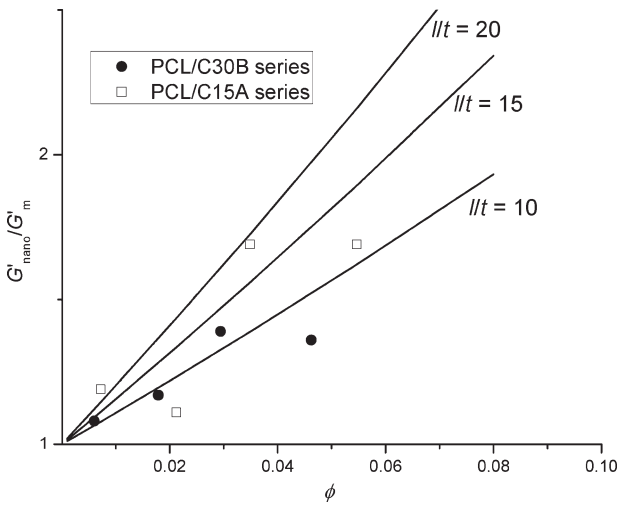

Figure 10. Comparison of the theoretical relative modulus as a function of the volume fraction obtained from the Halpin–Tsai model (solid lines) with experimentally observed values for the different nanocomposites (open and filled squares).

nanocomposites with two different organomodified clays were prepared by solution casting. With WAXD analysis, it was possible only to detect the presence of the clay with mostly unaltered interlayer distance in the both series of nanocomposites. The diffraction patterns indicated also a presence of a portion of intercalated clay in the case of nanocomposites with CloisiteC15A. The difference between the two series of the nanocomposites was significant in their melt rheological response. The melt rheological measurements showed that with the addition of the clay the complex viscosity progressively increases with the appearance of the shear-thinning behavior in the low frequency region. The melt yield stress values for the nanocomposites were determined using the Carreau–Yasuda model. Two to three orders of magnitude higher values for the yield stress exhibited by the nanocomposites' melt in the series with C15A clay were ascribed to the presence of a certain amount of the exfoliated clay. From the increase in the storage modulus of the melt the effective aspect ratio of the clay particles was estimated to be of the similar value for the both series of nanocomposites. The nanocomposites showed thermorheological simplicity and it was possible to apply the time-superposition principle. The temperature dependence of the applied horizontal shift factors for different nanocomposites, which was similar for all the samples, showed that relaxation processes in the molten nanocomposites are unaffected by the presence of the clay. Dynamic mechanical analysis in the solid state revealed that the glass transition temperature of the nanocomposites was not largely affected by the clay presence. The difference in the loss factor peak height and area between the two series of the nanocomposites was noticed and was ascribed to the presence of the fraction of exfoliated clay, deduced also from melt rheological data. The nanocomposites showed improved storage modulus particularly above, but also below the glass transition temperature. The improvement of mechanical properties—increase in the storage modulus of the solid nanocomposites, was correlated to the Halpin–Tsai semiempirical model predictions. Effective aspect ratios of the clays deduced from these correlations are comparable to the value obtained from melt rheological measurements. These findings show that mechanical properties are mainly influenced by the effective aspect ratio of the clay, which can be obtained from the rheological measurements in the melt.

ACKNOWLEDGMENTS

This work was financially supported by the Ministry of Education, Science and Technological Development of the Republic of Serbia (Project No. 172062).

REFERENCES

1. Woodruff, M. A.; Hutmacher, D. W. *Prog. Polym. Sci.* **2010**, *35*, 1217.
2. Bordes, P.; Pollet, E.; Averous, L. *Prog. Polym. Sci.* **2009**, *34*, 125.
3. Paul, D. R.; Robeson, L. M. *Polymer* **2008**, *49*, 3187.
4. Pavlidou, S.; Papaspyrides, C. D. *Prog. Polym. Sci.* **2008**, *33*, 1119.
5. Alexandre, M.; Dubois, P. *Mater. Sci. Eng. R* **2000**, *28*, 1.
6. Jimenez, G.; Ogata, N.; Kawai, H.; Ogihara, T. *J. Appl. Polym. Sci.* **1997**, *64*, 2211.
7. Lepoittevin, B.; Devalckenaere, M.; Pantoustier, N.; Alexandre, M.; Kubies, D.; Calberg, C.; Jérôme, R.; Dubois, P. *Polymer* **2002**, *43*, 4017.
8. Lepoittevin, B.; Pantoustier, N.; Devalckenaere, M.; Alexandre, M.; Kubies, D.; Calberg, C.; Jérôme, R.; Dubois, P. *Macromolecules* **2002**, *35*, 8385.
9. Kotek, J.; Kubies, D.; Baldrian, J.; Kovářová, J. *Eur. Polym. J.* **2011**, *47*, 2197.
10. Wu, T.; Xie, T.; Yang, G. *Appl. Clay Sci.* **2009**, *45*, 105.
11. Ludueña, L. N.; Alvarez, V. A.; Vazquez, A. *Mater. Sci. Eng. A* **2007**, *460461*, 121.
12. Pucciariello, R.; Villani, V.; Guadagno, L.; Vittoria, V. *J. Polym. Sci. Part B: Polym. Phys.* **2006**, *44*, 22.
13. Gorrasi, G.; Tortora, M.; Vittoria, V.; Pollet, E.; Lepoittevin, B.; Alexandre, M.; Dubois, P. *Polymer* **2003**, *44*, 2271.
14. Ludueña, L. N.; Vazquez, A.; Alvarez, V. A. *J. Appl. Polym. Sci.* **2008**, *109*, 3148.
15. Chrissafis, K.; Antoniadis, G.; Paraskevopoulos, K. M.; Vassiliou, A.; Bikiaris, D. N. *Compos. Sci. Technol.* **2007**, *67*, 2165.
16. Solomon, M. J.; Almusallam, A. S.; Seefeldt, K. F.; Somwangthanaroj, A.; Varadan, P. *Macromolecules* **2001**, *34*, 1864.
17. Krishnamoorti, R.; Giannelis, E. P. *Macromolecules* **1997**, *30*, 4097.
18. Li, Y.; Han, C.; Zhang, X.; Bian, J.; Han, L. *Polym. Compos.* **2013**, *34*, 1620.
19. Li, Y.; Han, C.; Bian, J.; Han, L.; Dong, L.; Gao, G. *Polym. Compos.* **2012**, *33*, 1719.
20. Kasgoz, A.; Akın, D.; Durmus, A. *J. Reinf. Plast. Compos.* **2012**, *31*, 1329.
21. Miltner, H. E.; Watzeels, N.; Block, C.; Gotzen, N. A.; Assche, G. V.; Borghs, K.; Durme, K. V.; Mele, B. V.; Bogdanov, B.; Rahier, H. *Eur. Polym. J.* **2010**, *46*, 984.
22. Százdi, L.; Ábrányi, Á.; Pukánszky, B.; Vancso, J. G.; Pukánszky, B. *Macromol. Mater. Eng.* **2006**, *291*, 858.
23. Cassagnau, P. *Polymer* **2008**, *49*, 2183.
24. Litchfield, D. W.; Baird, D. G. *Rheol. Rev.* **2006**, *1*.
25. Wagener, R.; Reisinger, T. J. G. *Polymer* **2003**, *44*, 7513.
26. Block, C.; Watzeels, N.; Rahier, H.; Mele, B.; Assche, G. *J. Therm. Anal. Calorim.* **2011**, *105*, 731.
27. Wu, D.; Wu, L.; Sun, Y.; Zhang, M. *J. Polym. Sci. Part B: Polym. Phys.* **2007**, *45*, 3137.
28. Kwak, S. Y.; Sei Oh, K. *Macromol. Mater. Eng.* **2003**, *288*, 503.
29. Ahmed, J.; Auras, R.; Kijchavengkul, T.; Varshney, S. K. *J. Food Eng.* **2012**, *111*, 580.
30. Tarkin-Tas, E.; Goswami, S. K.; Nayak, B. R.; Mathias, L. J. *J. Appl. Polym. Sci.* **2008**, *107*, 976.
31. Saeed, K.; Park, S. Y. *J. Appl. Polym. Sci.* **2007**, *104*, 1957.

32. Avella, M.; Bondioli, F.; Cannillo, V.; Pace, E. D.; Errico, M. E.; Ferrari, A. M.; Focher, B.; Malinconico, M. *Compos. Sci. Technol.* **2006**, *66*, 886.
33. Nikolić, M. S.; Đorđević, N.; Rogan, J.; Đonlagić, J. *J. Serb. Chem. Soc.* **2015**, *80*, 529.
34. Chen, B.; Evans, J. R. G. *Macromolecules* **2005**, *39*, 747.
35. Galgali, G.; Ramesh, C.; Lele, A. *Macromolecules* **2001**, *34*, 852.
36. Homminga, D.; Goderis, B.; Dolbnya, I.; Groeninckx, G. *Polymer* **2006**, *47*, 1620.
37. Kiersnowski, A.; Gutmann, J. S.; Pigłowski, J. *J. Polym. Sci. Part B: Polym. Phys.* **2007**, *45*, 2350.
38. Neppalli, R.; Causin, V.; Marega, C.; Saini, R.; Mba, M.; Marigo, A. *Polym. Eng. Sci.* **2011**, *51*, 1489.
39. Ren, J.; Silva, A. S.; Krishnamoorti, R. *Macromolecules* **2000**, *33*, 3739.
40. Lertwimolnun, W.; Vergnes, B. *Polymer* **2005**, *46*, 3462.
41. Lertwimolnun, W.; Vergnes, B. *Polym. Eng. Sci.* **2006**, *46*, 314.
42. Zachariah, A. K.; Geethamma, V. G.; Chandra, A. K.; Mohammed, P. K.; Thomas, S. *RSC Adv.* **2014**, *4*, 58047.
43. Kutlu, B.; Meinl, J.; Leuteritz, A.; Brünig, H.; Heinrich, G. *Polymer* **2013**, *54*, 5712.
44. Berzin, F.; Vergnes, B.; Delamare, L. *J. Appl. Polym. Sci.* **2001**, *80*, 1243.
45. Yuan, L.; Wu, D.; Zhang, M.; Zhou, W.; Lin, D. *Ind. Eng. Chem. Res.* **2011**, *50*, 14186.
46. Lee, K. M.; Han, C. D. *Macromolecules* **2003**, *36*, 7165.
47. Noroozi, N.; Thomson, J.; Noroozi, N.; Schafer, L.; Hatzikiriakos, S. *Rheol. Acta* **2012**, *51*, 179.
48. Chung, J. W.; Oh, K. S.; Kwak, S. Y. *Macromol. Mater. Eng.* **2007**, *292*, 627.
49. Ramkumar, D. H. S.; Bhattacharya, M. *Polym. Eng. Sci.* **1998**, *38*, 1426.
50. Acierno, S.; Di Maio, E.; Iannace, S.; Grizzuti, N. *Rheol. Acta* **2006**, *45*, 387.
51. Liu, Q.; Chen, D. *Eur. Polym. J.* **2008**, *44*, 2046.
52. Sinha Ray, S.; Okamoto, K.; Okamoto, M. *Macromolecules* **2003**, *36*, 2355.
53. Gu, S. Y.; Ren, J.; Dong, B. *J. Polym. Sci. Part B: Polym. Phys.* **2007**, *45*, 3189.
54. Harrison, K. L.; Jenkins, M. J. *Polym. Int.* **2004**, *53*, 1298.
55. Masenelli-Varlot, K.; Reynaud, E.; Vigier, G.; Varlet, J. *J. Polym. Sci. Part B: Polym. Phys.* **2002**, *40*, 272.
56. Marras, S. I.; Kladi, K. P.; Tsivintzelis, I.; Zuburtikudis, I.; Panayiotou, C. *Acta Biomater.* **2008**, *4*, 756.
57. Zhang, X.; Loo, L. S. *Macromolecules* **2009**, *42*, 5196.
58. Fernández, M.; Landa, M.; Muñoz, M. E.; Santamaría, A. *Macromol. Mater. Eng.* **2010**, *295*, 1031.
59. Fornes, T. D.; Paul, D. R. *Polymer* **2003**, *44*, 4993.
60. Arza, C. R.; Jannasch, P.; Maurer, F. H. *J. Eur. Polym. J.* **2014**, *59*, 262.
61. Lonjon, A.; Demont, P.; Dantras, E.; Lacabanne, C. *J. Non-Cryst. Solids* **2012**, *358*, 236.
62. Vlasveld, D. P. N.; de Jong, M.; Bersee, H. E. N.; Gotsis, A. D.; Picken, S. J. *Polymer* **2005**, *46*, 10279.
63. Faraz, M. I.; Besseling, N. A. M.; Korobko, A. V.; Picken, S. J. *Composites Part B* **2014**, *56*, 9.